Strong Acoustic Phonon Localization in Copolymer-Wrapped Carbon Nanotubes

Ibrahim Sarpkaya,[†] Ehsaneh D. Ahmadi,[†] Gabriella D. Shepard,[†] Kevin S. Mistry,[‡] Jeffrey L. Blackburn,[‡] and Stefan Strauf*[,†]

[†]Department of Physics & Engineering Physics, Stevens Institute of Technology, Castle Point on the Hudson, Hoboken, New Jersey 07030, United States and [‡]National Renewable Energy Laboratory, Golden, Colorado 80401, United States

ABSTRACT Understanding and controlling exciton−phonon interactions in carbon nanotubes has important implications for producing efficient nanophotonic devices. Here we show that laser vaporization-grown carbon nanotubes display ultranarrow luminescence line widths (120 μeV) and well-resolved acoustic phonon sidebands at low temperatures when dispersed with a polyfluorene copolymer. Remarkably, we do not observe a correlation of the zero-phonon line width with ^{13}C atomic concentration, as would be expected for pure dephasing of excitons with acoustic phonons. We demonstrate that the ultranarrow and phonon sideband-resolved emission spectra can be fully described by a model assuming extrinsic acoustic phonon localization at the nanoscale, which holds down to 6-fold narrower spectral line width compared to previous work. Interestingly, both exciton and acoustic phonon wave functions are strongly spatially localized within 5 nm, possibly mediated by the copolymer backbone, opening future opportunities to engineer dephasing and optical bandwidth for applications in quantum photonics and cavity optomechanics.

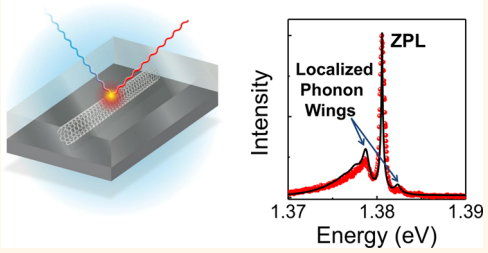

KEYWORDS: carbon nanotubes · excitons · acoustic phonon localization · isotope effects · dephasing

Single-walled carbon nanotubes (SWCNTs) are well-known for their applications in nanoelectronics and have gained tremendous interest as a nanomaterial for next generation optoelectronics and quantum photonic devices.[1−4] A key feature that sets SWCNTs apart from common compound semiconductors is their large exciton binding energy that reaches up to 400 meV,[5] more than an order of magnitude larger than the thermal energy at room temperature. While emission from the visible to near-infrared regions including all telecom bands is possible, the often-reported low photoluminescence (PL) quantum yield of SWCNTs constitutes a severe drawback.[6] Low efficiencies can result from extrinsic interactions with the nanotube environment, which leads to nonradiative recombination (NR) as highly mobile excitons explore defects and dopants along the tube.[7−14] The corresponding exciton spontaneous emission (SE) lifetimes are typically measured to be rather short with values of T_1 = 20−200 ps.[3,8,10,15,16] These short lifetimes due to dominant NR imply strongly reduced optical emission rates of nanoscale light sources. Likewise, high NR rates lead to reduced light-to-current conversion efficiencies in photodetectors or solar cells that are based on SWCNTs.

Recent efforts aiming to overcome these deficiencies have utilized "ultraclean" SWCNTs that are suspended over an air gap.[17,18] Air-suspended SWCNTs are often said to be ultraclean to reflect reduced disorder in the absence of a substrate, which facilitates the observation of phenomena such as Wigner crystallization,[19] spin−orbit coupling,[20] and the Mott insulating state.[18] We have demonstrated that such ultraclean SWCNTs feature drastically prolonged SE lifetimes up to T_1 = 18 ns,[17] while Hoffmann *et al.* reported comparable SE times up to 4 ns.[21] These prolonged SE lifetimes are in agreement with values predicted a decade ago for idealized SWCNTs that are not affected by environmental interactions.[22,23] One could thus consider that the optical emission of these ultraclean

* Address correspondence to strauf@stevens.edu.

Received for review April 2, 2015 and accepted June 3, 2015.

Published online June 03, 2015
10.1021/acsnano.5b01997

air-suspended SWCNTs has reached an "intrinsic regime", where the optical properties are no longer affected by the nanotube environment.

In addition to efficient emission, quantum optical devices also require long exciton dephasing times (T_2 times) to realize, for example, Fourier transform (FT) limited emission of indistinguishable single photons. This can be achieved if dephasing is purely defined by radiative decay, corresponding to the condition $T_2/2T_1 = 1$. In earlier work, studies of the exciton dephasing time for large ensembles of SWCNTs revealed extremely short T_2 values of about 500 fs at 4 K, which were in agreement with the ensemble PL line width of about 7 meV in these samples.[24,25] These ultrafast T_2 times are 2−3 orders of magnitude smaller than the corresponding T_1 times, leaving the exciton emission of SWCNTs far from being FT limited.

The underlying exciton−phonon coupling is at the heart of exciton dephasing and was theoretically described by Galland *et al.*[26] using an Ohmic interaction model that describes the deformation potential interaction of zero-dimensional (0D) excitons that are spatially localized along the nanotube, with idealized one-dimensional (1D) acoustic phonons of stretching modes seeking agreement with the often observed broad PL line width of individual SWCNTs of several millielectronvolts.[26,27] The recent discovery of an ultranarrow exciton line width regime of individual air-suspended SWCNTs with best case zero-phonon line width (ZPL) values of 220[17] and 40 μeV[21] challenges the Ohmic model, assuming coupling to 1D phonons that apparently largely overestimates the exciton−acoustic phonon interaction. These experiments also revealed prolonged T_2 times of individual SWCNTs, either directly measured with T_2 values up to 2.1 ps[17] or inferred from time-integrated spectra implying a lower bound for T_2 of at least 15 ps,[21] which is 30 times longer than that observed in early ensemble studies of surfactant-dispersed SWCNTs.[24,25]

In light of these recent findings, questions arise regarding the actual mechanism of exciton−phonon interaction and if the dephasing is intrinsic to the SWCNTs or caused by extrinsic effects that could possibly be engineered toward longer T_2 times. To this end, we demonstrated that the time-integrated spectral line width Γ of ultraclean SWCNTs is not necessarily dominated by pure dephasing with acoustic phonons since line width measurements of the ZPL width Γ are always found to be larger than values that can be calculated using the well-known relation $\Gamma = \hbar/T_1 + 2\hbar/T_2$ and directly measured exciton SE and dephasing times, implying that an additional mechanism(s) must affect the exciton line width.[17] One possible extrinsic candidate is spectral diffusion that can additionally broaden the time-integrated ZPL width where charge fluctuations in the SWCNT vicinity contribute to dynamical Stark shift broadening. Another extrinsic mechanism was recently introduced by Vialla *et al.* and is based on the idea that the acoustic phonon modes can be spatially localized along the nanotube due to acoustic barriers with energies of a few millielectronvolts and spatial phonon localization length of up to 35 nm.[28] This model gave good agreement with ZPL width down to 700 μeV. Since the phonons no longer have the 1D characteristic predicted by the Ohmic model but behave rather like being 0D, one can refer to this case as the non-Ohmic model.

It is an open question if the non-Ohmic model holds down to the ultranarrow line width regime, in particular, since attempts to fit the highly symmetric and ultranarrow exciton spectra of air-suspended SWCNTs need to assume T_2 times that are significantly longer than experimental values.[28] In addition, from a device point of view, one would also like to be able to embed SWCNTs in a matrix material, for example, to couple them to dielectric or plasmonic cavities, while ideally preserving the ultranarrow line width and prolonged exciton dephasing times found in air-suspended nanotubes.

Here we demonstrate that polymer-matrix-embedded individual SWCNTs can indeed reach deeply into the ultranarrow line width regime with zero-phonon line width values down to 120 μeV. This was accomplished utilizing laser vaporization growth of small-diameter SWCNTs combined with polyfluorene wrapping for selective dispersion of semiconducting nanotubes that are further embedded in a nonpolar polystyrene matrix to effectively eliminate spectral diffusion. To investigate the underlying microscopic mechanism of the exciton−phonon interaction, we directly aimed to manipulate the phonon density of states utilizing isotope engineering of SWCNTs with various ^{13}C compositions. While it is expected that the exciton dephasing time should be reduced in the presence of the heavier ^{13}C atoms with finite nuclear spin, our data show no clear dependence of line shape on $^{13}C/^{12}C$ isotopic ratios despite the remarkably narrow spectral line width. We also show evidence that impurity-bound exciton emission can be ruled out. These observations indicate that the spectral line shape is not solely affected by the deformation potential interaction of excitons with idealized 1D acoustic phonons. In addition, we show that the exciton emission spectra in the ultranarrow line width regime feature spectrally resolved phonon sidebands following a characteristic pump power and temperature dependence for copolymer-wrapped SWCNTs, while surfactant-dispersed SWCNTs feature only a rather broad exciton line width. These temperature-dependent line shapes can be theoretically described by introducing acoustic phonon mode confinement, inducing energy gaps in the phonon density of states. Our findings imply that exciton dephasing and spectral line shape of semiconducting SWCNTs are strongly

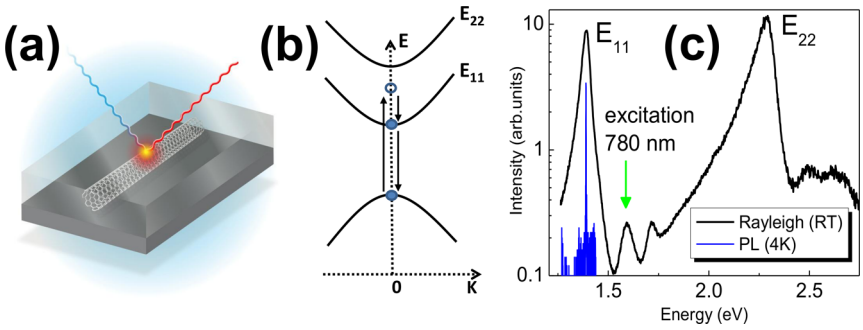

Figure 1. Polymer-embedded SWCNT device structure and quasi-resonant excitation scheme. (a) Schematic diagram of an individual SWCNT deposited between two polymer layers suspended above a Au-coated substrate. (b) Schematic of quasi-resonant pumping of excitons into their excited states *via* one-phonon absorption processes involving the zone-center optical phonons. (c) Rayleigh spectrum of an individual (6,4) chirality tube at room temperature (black line) with a 4 K PL spectrum (blue line).

affected by extrinsic acoustic phonon localization effects, likely mediated by the copolymer wrapping.

RESULTS AND DISCUSSION

The first goal of our study was to isolate individual SWCNTs with known chirality, targeting, in particular, semiconducting carbon nanotubes with (6,4) chirality emitting at 890 nm from an ensemble of SWCNTs grown by the laser vaporization (LV) technique (see Methods). Access to individual SWCNTs was facilitated by depositing small quantities of SWCNTs dispersed with a polyfluorene polymer (PFO-BPy) in toluene solution onto a substrate. It is well-known that uncapped surfactant-dispersed SWCNTs on a SiO_2 wafer suffer typically from strong environmental interactions such as spectral diffusion and blinking. To avoid this, we followed our previous work where we demonstrated that these detrimental effects on the exciton emission can be strongly suppressed by embedding SWCNTs in a polystyrene (PS) matrix of a thin-slab half-cavity, leading to 50-fold enhanced light collection.[4,29] In addition, a very recent study showed that PFO wrapping is preferred compared to other surfactant wrapping techniques because it leads to spectrally narrow exciton emission spectra.[30]

Figure 1a shows a schematic of the sample design consisting of a bottom gold mirror, a PS spacer, a dispersed SWCNT layer, and a top PS capping layer. To predominantly excite (6,4) chirality SWCNTs that are known to emit at 890 nm (1.39 eV), we utilized phonon-assisted excitation around 780 nm (1.59 eV), which results in quasi-resonant pumping of excitons into their excited states *via* one-phonon absorption processes involving the zone-center optical phonons[31] (G-mode phonon with energy of about 200 meV), as illustrated in Figure 1b. After excitation, the excitons relax nonradiatively from their excited state into the E_{11} ground-state exciton level *via* emission of a single zone-center optical phonon, from where they decay radiatively into the ground state with PL emission around 890 nm. Unlike the typical pumping of SWCNTs into the higher energetic E_{22} electronic states, this quasi-resonant excitation scheme avoids multiphonon-assisted exciton relaxation processes. It is expected that this leads to a more direct optical excitation of the excitons, similar to the p-shell pumping of semiconductor quantum dots displaying strongly reduced multiphoton contributions, such as background-free single-photon emission in quantum optical measurements under quasi-resonant excitation into the excited exciton states.[32,33] The corresponding room temperature Rayleigh scattering spectrum in Figure 1c recorded for a (6,4) chirality SWCNT shows that a pronounced excitation channel around 780 nm is indeed present between the characteristic E_{11} and E_{22} transitions.

Since the chirality of the SWCNTs cannot be easily controlled in the laser vaporization growth process, there are two possible cases for the observed signal at 890 nm under quasi-resonant excitation at 780 nm. If a (6,4) chirality SWCNT is indeed present in the excitation spot, then one expects to find PL emission from excitons at 890 nm, while for all other chiralities, and in particular for metallic tubes, one expects the Raman G-band signature instead. Previously, one could distinguish Raman and PL signals from individual SWCNTs simply based on the spectral line width. At typical G-band line widths of about 1 meV, corresponding to rather fast phonon decay times of about 2 ps,[34−37] the Raman signal was found to be much narrower than typical exciton emission spectra. However, the recent observation of extremely narrow spectral exciton line widths in ultraclean SWCNTs[17,21] makes this assumption no longer reliable. Therefore, in order to differentiate PL from Raman, we carried out spectral detuning experiments of the excitation wavelength of the pump laser (see Methods section), as shown in Figure 2.

In the first case shown in Figure 2a, the optical spectrum follows the spectral shift of 6 meV of the tunable excitation laser. When plotted as an inelastic light scattering spectra (energy shift relative to the

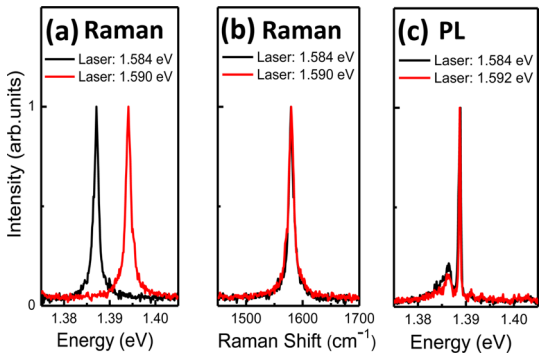

Figure 2. Differentiation of PL from Raman by detuning the excitation wavelength of the pump laser. (a) Raman spectra of an individual SWCNT for two different excitation wavelengths plotted *versus* energy. (b) Raman spectra of the same tube in (a) plotted as an inelastic light scattering spectrum. (c) Spectra taken from another SWCNT for comparable laser detuning energies like in (a,b). The lack of a spectral shift for excitation detuning and the absolute emission energy reveal this case as PL rather than Raman emission from a (6,4) SWCNT. Note the appearance of a peculiar low-energy wing in such PL spectra recorded at 9 K.

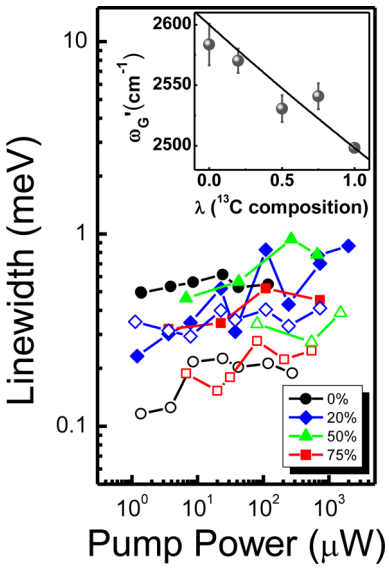

Figure 3. Spectral line width study for different carbon isotope compositions. Lorentzian line width values *versus* pump power for PFO-dispersed and polymer-embedded SWCNTs with "pure" ^{12}C (black circles), 20% ^{13}C (blue diamonds), 50% ^{13}C (green triangles), and 75% ^{13}C (red squares) admixing of ^{13}C during growth. The solid and open symbols distinguish two representative data sets for each isotope composition. Inset: Plot of G′ Raman band frequency as a function of ^{13}C composition recorded from individual SWCNTs. Each data point (gray circles) represents the average experimental value of the G′ frequency of 3−10 tubes. The error bars correspond to statistical variations for each data point. The black solid line is the expected Raman mode softening based on the varying carbon atom mass that follows the equation given in the main text. Data are recorded at 9 K.

incident laser wavelength), both spectra are on top of each other, which clearly identifies the signal to be of Raman origin (Figure 2b). The absolute energy loss of 1590 cm^{-1} is in excellent agreement with the G-mode phonon energy (200 meV). In contrast to the case described in Figure 2a,b, we also identify many individual SWCNTs by laterally scanning the sample under the laser spot and showing that there is no spectral shift even for laser detuning up to 8 meV, as shown in Figure 2c. In this case, the optical emission is caused by spontaneous emission from quasi-resonantly excited excitons that seem to dominate over a possible Raman signal. The absolute emission energy of 1.388 eV (890 nm) is also in excellent agreement with the known PL emission from (6,4) chirality SWCNTs.[38] Furthermore, the PL emission in these LV-grown and PFO-dispersed samples is significantly narrower than the Raman signatures, that is, the exact opposite from earlier findings in SWCNTs showing strong exciton line width broadening due to environment interaction.[39] With this clear separation of pure Raman signals from exciton emission, we investigated the PL emission in more detail with a particular focus on the additional low-energy wing around 1.386 eV that can be seen in Figure 2c.

Figure 3 shows the corresponding full width at half-maximum (fwhm) line width values extracted from simple Lorentzian line shape fits that neglect the low-energy wing for various pump powers and carbon isotope compositions. The corresponding spectral line width of the dominant PL peak in these LV-grown SWCNTs is, with values down to 120 μeV, significantly narrower than that in most reports in the literature[4,24−29,39,40] and comparable to very recent demonstrations in free-standing SWCNTs[17,21] as well as PFO-dispersed SWCNTs.[30]

To further investigate the underlying microscopic mechanism, we have considered three possible effects that can contribute to the exciton emission spectra and the ZPL width, in particular. (i) If the exciton spectrum is dominated by dephasing with intrinsic 1D acoustic phonons, it should be sensitive to the carbon isotope composition that directly affects the phonon density of states (Ohmic model). (ii) If the spectrum is dominated by impurity-bound exciton emission instead of exciton−phonon interactions, it should follow characteristic spectral distributions. (iii) If it is dominated by dephasing with extrinsically localized phonons, it should show well-resolved phonon sidebands and characteristic pump power and temperature behavior (non-Ohmic model). In the following, we provide evidence that exciton emission line shapes in our copolymer-wrapped samples are dominated by non-Ohmic phonon localization effects rather than by pure dephasing with 1D acoustic phonons or by impurity-bound excitons.

To directly manipulate the phonon density of states, we utilized isotope engineering of SWCNTs with various ^{13}C compositions and studied the exciton PL line width down to lowest pump powers, where contribution to dephasing from exciton−exciton scattering is minimized. Specifically, samples were grown with

carbon isotope compositions varied from the natural ^{12}C ratio (1% ^{13}C) to 20, 50, 75, and 100% admixing of ^{13}C (see Methods section). As a first test to determine if the growth was carried out successfully, we measured the isotope effect on the phonon energies for individual SWCNTs. The inset in Figure 3 shows an example Raman shift of the G′ band (2590 cm^{-1}) as a function of ^{13}C composition averaging data from 3 to 10 tubes in each case. Replacement of ^{12}C atoms with the ^{13}C atoms results in a downshift of the G′ frequency due to the vibrational softening caused by the heavier ^{13}C mass. This can be quantified by the relation of the phonon frequency ω_0 at the Brillouin zone center in pure ^{12}C to the phonon frequency $\omega(\lambda)$ in nanotubes doped with ^{13}C at a concentration of λ, which is given by

$$\frac{\omega(\lambda)}{\omega_0} = \sqrt{\frac{M^{12}C}{\lambda M^{13}}C + (1 - \lambda)M^{12}C}$$

where M is the mass of the respective isotopes (solid line in Figure 3 inset).[41] While the data follow the trend quite well, remaining variations are likely caused by the varying degree of residual strain from tube to tube[42] and/or the different amount of chirality-dependent phonon frequency shifts.[43] The observed isotope shift for individual SWCNTs is also in excellent agreement with previous findings carried out with large ensembles of SWCNTs from the same LV growth chamber[44,45] as well as chemical vapor deposition grown SWCNTs.[46]

For these isotope-engineered SWCNTs, the signature of exciton emission was confirmed in each case by the laser detuning technique described in Figure 2, with yields of about 10−30% for finding (6,4) chirality SWCNTs, with the exception of the 100% ^{13}C samples, where we found no PL signal around 890 nm that would correspond to (6,4) chirality but only the Raman G band signatures from SWCNTs with other chiralities. The line width data in Figure 3 vary by about 1 order of magnitude with values ranging from 0.1 to 1 meV. The solid and open symbols distinguish two representative data sets for each isotope composition. Note that the ZPL width for some SWCNTs seems to be largely unaffected by the change in pump power over 3 orders of magnitude (*e.g.*, the open blue diamonds for 20% ^{13}C admixing). This is an indication that the ZPL width of these SWCNTs is pinned to extrinsic effects. However, most of the studied SWCNTs and, in particular, those featuring the narrowest ZPL width show a systematic ZPL broadening that can be attributed to pump-power-induced pure dephasing. The data show no general trend with isotope tuning since one can find examples of both ^{12}C and 75% ^{13}C carbon nanotubes that feature spectral line widths that are either ultranarrow with values of about 120−200 μeV or significantly broader with values approaching 600 μeV.

If the exciton emission would be dominated by pure dephasing with 1D acoustic phonons, one would expect the line width to systematically broaden with the admixing of ^{13}C. First of all, it is well-known that the electron-spin coherence time in the presence of ^{13}C is strongly reduced due to the hyperfine interaction of their nuclear spin of 1/2.[47,48] In contrast, SWCNTs grown from purified ^{12}C sources possess a nuclear spin of zero. Thus, theoretically, the absence of a hyperfine interaction in a nearly spin-free lattice would result in ultralong spin coherence times for ^{12}C-purified SWCNTs and diamond, making these materials promising candidates for spin-qubits. Likewise, the exciton dephasing time is expected to be reduced in the presence of ^{13}C since the deformation potential coupling of the underlying exciton−acoustic phonon interaction is stronger when the mass of the carbon atoms is heavier, as is evident from the 1D phonon density of states, which is proportional to the square root of the carbon mass.[49] The fact that we find no clear trend with isotope tuning in the data of Figure 3 indicates that the exciton emission spectrum is not dominated by pure exciton dephasing with 1D acoustic phonons. These data provide an upper bound for the contribution of ^{13}C-induced dephasing to the ZPL of about 200 μeV.

To probe for the possibility of impurity-bound exciton emission from excitons localized at unintentional dopant sites or defects, we investigated the E_{11} emission spectra of 48 SWCNTs. Figure 4 displays the low

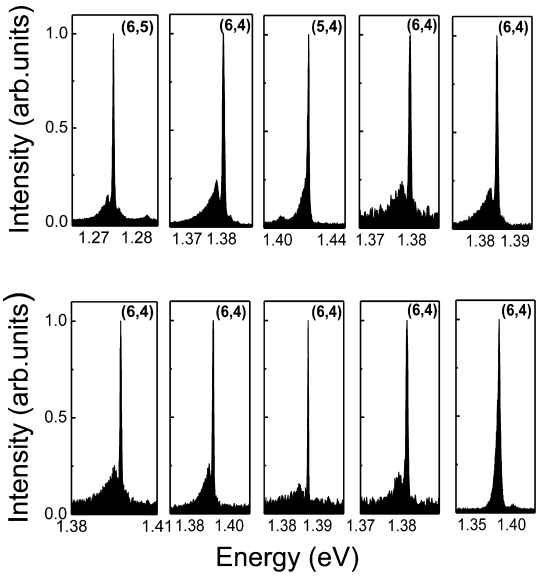

Figure 4. Comparison of phonon sidebands in PL spectra of individual SWCNTs with various isotope compositions. The 10 PL spectra shown are representative for experimental findings of about 48 measured SWCNTs. In all cases, including three different chiralities of (5,4), (6,4), and (6,5) SWCNTs, only one dominant emission line as well as pronounced asymmetry to lower energies is found. While most cases show a spectrally resolved phonon sideband separated from the main peak by 2−4 meV, some of the SWCNTs feature a side wing that is smoothly merged with the E_{11} transition. Chirality of each tube is indicated in parentheses. Data are recorded at low pump power and 9 K.

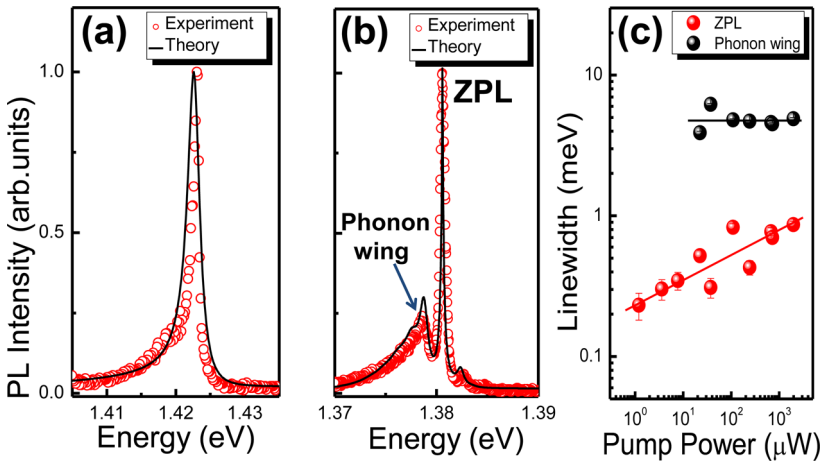

Figure 5. Comparison of theory line shape with measured PL spectra. Open circles show measured data from two individual SWCNTs for (a) (5,4) chirality and (b) (6,4) chirality. The black solid lines are the calculated spectra considering the Ohmic (a) and non-Ohmic (b) model of exciton−phonon interaction, respectively. ZPL: Zero-phonon line. (c) Pump-power-dependent line width of the ZPL as well as the spectrally resolved phonon wing. Data are recorded at 9 K.

pump power spectra of 10 individual SWCNTs for three different chiralities, including (6,4), (6,5), and (5,4) SWCNTs. We note that the pump power for the quasi-resonant phonon sideband excitation was deliberately kept low enough ($\leq$1 mW/μm^2) to avoid optically induced damage that is known, in particular, for E_{22} excitation, to induce blinking[30,50] and additional defect-related exciton emission lines.[30,51−54] In all cases, we found only one dominant emission line as well as a pronounced asymmetry to lower energies featuring a wing that is either separated from the main peak by 1−4 meV or smoothly merged with the E_{11} transition. Importantly, in all cases, the intensity of the wing is in the range of 15−22% of the E_{11} ZPL intensity for spectra taken at 9 K.

These findings are in contrast to recent results of intentionally oxygen-doped SWCNTs that feature splitting of the E_{11} transition into three peaks with much larger splitting energies of about 7 and 19 meV, as well as strongly varying intensity ratios with some cases of a dominant high-energy peak and others with a dominant low-energy peak.[55] In that work, undoped reference samples featured only one dominant peak in the E_{11} regime as in our case, albeit with a broad line width of about 4 meV. Based on these distinct differences, and the fact that our samples did not undergo any intentional oxygen doping, we rule out oxygen-dopant-bound exciton emission as the cause for the low-energy PL wings in Figure 4. Furthermore, recent magneto-PL experiments of individual PFO-dispersed SWCNTs not exposed to irradiation damage show that zero-field spectra display also only one exciton emission line, like in our spectra, while high-field spectra show many lines related to exciton localization effects as well as dark-state brightening.[30] We further note that it is evident that the exciton wave function in SWCNTs is spatially localized in slowly varying local potentials at low temperatures, even in the absence of magnetic fields, as demonstrated by pronounced photon antibunching signatures, indicating that zero-dimensional quantum-dot-like exciton states are frequently formed at low temperatures.[4,17,21]

Our findings in Figure 4 are also in contrast with our previous work on individual acceptor-bound exciton emission centers in semiconductors (*e.g.*, nitrogen-doped ZnSe), where the transition from the ensemble to individual localized dopant centers shows clearly that cases exist with one, two, or more impurity-bound exciton emission lines that have almost equal spectral intensities, each displaying photon antibunching.[56,57] A scenario of impurity-bound exciton emission at randomly distributed dopant atoms in our SWCNTs is thus rather unlikely in light of the fixed intensity ratio of the low-energy wing in 9 K spectra and the fact that we observe only one dominant PL peak, but never two or three, under low pump power conditions.

With impurity-bound exciton emission ruled out as the source of the observed low-energy PL wings, we now turn to the possibility of acoustic phonon localization (non-Ohmic model). As discussed below, our simulations demonstrate that the observed low-energy wings, the ultranarrow ZPL line width values, and the tube-to-tube variations can all be fully described by a mechanism combining the effects of exciton localization as well as disorder-induced acoustic phonon localization along the tube. The first case in Figure 5a shows an exciton emission spectrum for an individual (5,4) SWCNT with an asymmetric PL line shape, where the side peak is completely merged with the ZPL (open circles). This type of PL spectrum has been described under the assumption of Ohmic coupling of localized excitons to 1D acoustic phonons within the independent Boson model, that is, by the case without phonon confinement introduced by Galland *et al.*[26] The PL emission line shape function of QD-like excitons can be calculated by taking the

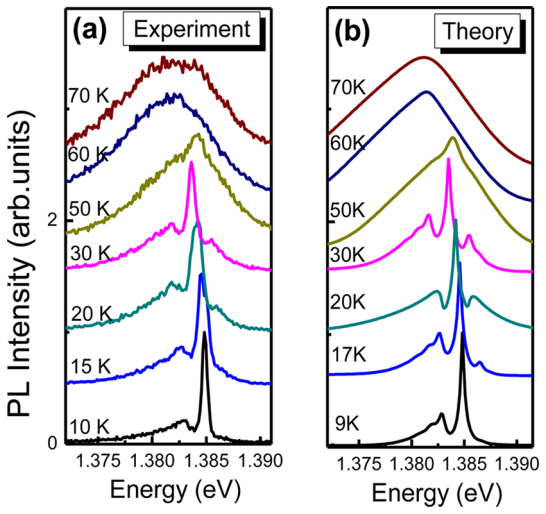

Figure 6. Temperature-dependent photoluminescence line shape study. Temperature dependence of measured PL spectra (a) and corresponding calculated PL spectra (b) considering the non-Ohmic model of exciton−phonon interaction. Excellent fits are made for an acoustic phonon confinement length of 4 ± 2 nm and an exciton wave function confinement of 3.3 ± 0.5 nm. Symmetrically spaced phonon side wings are observed that strongly vary their relative intensity with increasing temperature, in excellent agreement with predictions of the thermalization behavior of the bosonic phonon occupation number.

mirror image of the QD absorption spectrum, which is derived from the imaginary part of the Fourier transform of the linear susceptibility $\chi(t)$ in response to a δ-shaped laser pulse. The susceptibility $\chi(t)$ is proportional to the exciton−phonon coupling matrix element $g(q)$ that is given by the product of the exciton form factor $F_0(q)$, describing coupling of localized excitons in momentum space, and the deformation potential coupling $G(q)$ that depends, among other parameters, on the linear phonon dispersion $\omega(q) = v_s q$ of the stretching mode, where $v_s = 2 \times 10^4$ m/s is the velocity of sound. Best fits were obtained in Figure 5a for an exciton confinement length of $\sigma = 3.1 \pm 0.5$ nm. These values correspond to a localized exciton energy level splitting of $\Delta E = \hbar^2/M_x\sigma^2 = 39.5$ meV, where $M_x = 0.2$ is the effective exciton mass in units of the free electron mass (see Supporting Information).

Although the idealized Ohmic model follows the *qualitative* trend quite well, it overestimates the spectral line width with best-fit values for the fwhm of about 2 meV, while the experiment is about 1 meV. We note that this model, assuming idealized 1D phonons, has previously found excellent fit only with rather broad experimental spectra of about 4−6 meV fwhm.[26,28] For other cases shown in Figure 4 and in particular in Figure 5b and Figure 6, the Ohmic model completely fails because it cannot predict the formation of well-resolved acoustic phonon side wings or ultranarrow ZPL line width values.

In contrast, excellent fit to the peculiar exciton PL spectra can be achieved, as shown in Figure 5b, under the assumption that the acoustic phonon modes are confined between two acoustic barriers, here with a height of 1.6 meV and a phonon confinement length scale of $d = 4.5 \pm 2$ nm, while other parameters are kept comparable to the Ohmic model. This idea of confining acoustic modes was very recently introduced by Vialla *et al.* for the case of CoMoCat-grown SWCNTs that were dispersed in sodium cholate, resulting in 6-fold broader fwhm of about 700 μeV in the best case.[28] It can be technically implemented by making tiny modifications to the form factor $F_0(q)$ in the Ohmic model to account for an apparent environment-mediated low-energy cutoff in the acoustic phonon density of states (see Supporting Information). Since the phonons no longer have 1D character, like in the Ohmic model, but behave rather like being confined in all three dimensions (0D), we refer to this case as the non-Ohmic model. As a result, the fits to the experimental data in Figure 5b with the non-Ohmic model can fully describe the peculiar exciton line shapes. Importantly, this model can also make an excellent fit to the spectra with merged phonon sidebands shown in Figure 5a without overestimating the ZPL width (not shown).

To further validate the applicability of the non-Ohmic model, we probed the dependence of the ZPL and phonon wing peak widths on pump power. Increasing the optical pump power creates a higher exciton density, which leads to enhanced dephasing due to effects such as exciton−exciton scattering. According to the non-Ohmic model, the phonon wings should depend very weakly on dephasing (*i.e.*, pump-power-independent), while the ZPL should broaden considerably with the stronger dephasing induced by higher pump powers.[28] Figure 5c shows that this trend is nicely reproduced with a ZPL fwhm that triples with increasing pump power while the side peak width is nearly constant. Furthermore, it is found that the non-Ohmic model can fully describe the temperature-dependent spectra, as shown in Figure 6. The general trend of a strongly broadened line width with increasing temperature is well reproduced. Ultimately, spectra merge into a single nearly symmetric line shape above 50 K (k_BT = 4.3 meV) when the thermal energy is significantly larger than the acoustic barrier height. Both experiment and theory also show that an additional high-energy wing exists, corresponding to the anti-Stokes replica of the ZPL line (low-energy wing is the Stokes replica), as expected from the temperature dependence of the phonon occupation number. The relative height of the Stokes and anti-Stokes acoustic phonon wings is, as expected, found to follow a Boltzmann activation energy which is nearly equal to energy splitting of about 2 meV between each peak and the ZPL (see Supporting Information). Such a peculiar temperature dependence of the zero-phonon line and its side peaks is unlikely to be caused by other effects such as spectral diffusion or

localization of excitons at randomly distributed dopant atoms.

Interestingly, it appears that both exciton and acoustic phonon wave functions in polyfluorene-dispersed LV-grown SWCNTs are confined at the same length scale with values below 5 nm at 10 K. It is thus interesting to speculate about the underlying cause of acoustic phonon localization. To this end, it is striking that the same LV-grown SWCNTs if dispersed with sodium dodecylbenzenesulfonate (SDBS) display rather broad line width values about 2 meV or larger; that is, they do not enter the ultranarrow line width regime and have no apparent spectrally resolved side wings (see Supporting Information Figure S.1). We further note that the majority of our investigated PFO-BPy-dispersed SWCNTs (about 70−80%) display distinct phonon sidebands that are fully described by the non-Ohmic model assuming two acoustic barriers. Our findings are in contrast to the recent study by Vialla *et al.*,[28] reporting that less than 10% of the SWCNTs fall in this category of spectrally resolved sidebands, while most of their SWCNTs display asymmetric line shapes with fully merged low-energy wings, similar to observations by Galland *et al.*[26] The SWCNTs reported in ref 28 are based on CoMoCAT material that typically undergoes rigorous acid purification and was furthermore dispersed with sodium cholate, leading to the best ZPL line width values of about 700 μeV. In contrast, the LV-grown SWCNTs employed in this study did not undergo any purification and are therefore expected to have a defect density lower than that of the acid-purified CoMoCAT SWCNTs. Furthermore, dispersion with PFO-BPy in a low dielectric solvent (toluene rather than water) and subsequent embedding in PS results in better protection from detrimental environment effects, resulting in 6-fold narrower ZPL width of 120 μeV with pronounced phonon side wings at an intensity ratio of 0.15−0.22 with respect to the ZPL. Another important comparison can be made regarding the required phonon confinement length to fit the spectra in ref 28, which has values of up to $d = 35$ nm, significantly larger than our finding of $d = 4.5 \pm 2$ nm. This indicates that the phonon confinement is much stronger when SWCNTs are dispersed with PFO-BPy copolymer as compared to sodium cholate or SDBS. The choice of dispersant and solvent is thus key to uncovering the strong acoustic phonon localization regime in our work.

It is also apparent that the extrinsic localization is rather unlikely of pure random nature because the data fit quite well with a *single-phonon confinement length* rather than a broad distribution of confinement lengths, as one would expect for random disorder. Such a regular order could potentially represent a structure associated with the PFO-BPy copolymer, in particular, since there has been evidence in molecular dynamic simulations that PFO wraps helically around the SWCNT,[58,59] implying a fixed skipping distance at the nanoscale. It is thus considerable that the presence of a regularly spaced polymer backbone on top of the SWCNT can induce strong exciton and/or phonon confinement at the sub-10 nm length scale.

CONCLUSIONS

In summary, we have demonstrated that a mechanism of incorporating acoustic phonon localization at the nanometer length scale due to acoustic barrier heights of about 1−2 meV can fully account for the observed variety of asymmetric exciton emission spectra as well as their characteristic temperature-dependent phonon sidebands that appear spectrally resolved in the ultranarrow line width regime of copolymer-wrapped SWCNTs. We have shown that the non-Ohmic model holds well down to fwhm values of 120 μeV for the zero-phonon line, which are about 6-fold narrower compared to previous work. Despite the remarkably narrow ZPL width, we find no clear evidence from isotope tuning experiments that the nuclear-spin-mediated exciton dephasing in ^{13}C-containing SWCNTs contributes significantly to the spectral line shape, with an upper bound of 200 μeV. As such, exciton dephasing and spectral line shape of semiconducting SWCNTs in the ultranarrow line width regime are dominated by extrinsic acoustic phonon localization effects, likely mediated by the copolymer backbone. In future work, one can envision manipulation of the SWCNT environment in a more controlled way, for example, by wrapping SWCNTs with a regular array of copolymer strands of known length scale, to deliberately localize both excitons as well as acoustic phonons in predefined locations along the SWCNTs, thereby directly engineering the exciton−phonon interaction strength and thus the dephasing times and emission spectra for various applications in CNT quantum photonics and on-chip cavity optomechanics.

METHODS

SWCNT Synthesis. SWCNTs with the natural isotope ratio (99% ^{12}C) were synthesized by the laser vaporization process, as described previously.[60] The small-diameter SWCNTs synthesized for this study were produced at a furnace temperature of 800 °C in the LV process, and all syntheses were run at a power density of ~100 W/cm^2 (λ = 1064 nm, Nd:YAG). The target for all SWCNT syntheses containing ^{12}C consisted of Alfa Aesar graphite (2−15 μm, stock #14736), and all laser targets contained 3 wt % each nickel and cobalt catalysts. Targets for isotope-labeled SWCNTs were prepared with varying levels of amorphous ^{13}C (Cambridge Isotopes, 99% ^{13}C). Targets for SWCNTs labeled with 20−75% ^{13}C were prepared by mixing the appropriate amounts of graphitic ^{12}C, amorphous ^{13}C, and Ni/Co

catalysts, along with a small amount of ~5 wt % Carbowax aqueous solution.[44,45] The Carbowax is not needed for targets comprised of purely graphitic ^{12}C but serves as a binder for the ^{13}C targets since the amorphous ^{13}C does not bind well when compressed. The $^{12}C/^{13}C$ target mixture is ball-milled for 15 min before being compressed into a target. Once the $^{12}C/^{13}C$ target is placed into the quartz tube reaction chamber, the target is baked out at 1125 °C in a flowing N_2 (150 sccm) for 1 h to expel the majority of the Carbowax binder. This bake-out step is unnecessary for the graphitic ^{12}C target. Following bake-out, the furnace temperature was decreased to 800 °C and syntheses were run at a N_2 flow rate of 150 sccm and a total system pressure of 500 Torr. For the 100% ^{13}C target, we utilized only the amorphous ^{13}C and 3 wt % each nickel and cobalt catalysts. A 100% ^{13}C target was prepared on a purged ceramic press (with graphite compression rod) capable of maintaining high pressure and temperature. The amorphous ^{13}C in the ^{13}C/Co/Ni target was graphitized by holding the press at a temperature of ~2000 °C and a pressure of ~10 000 psi for 2 h while under inert purging conditions. This technique is similar to that employed by Stürzl *et al.*[61] SWCNTs were dispersed in poly[(9,9-dioctylfluorenyl-2,7-diyl)-*alt*-*co*-(6,60-{2,20-bipyridine})] (PFO-BPy) as discussed previously.[60] Briefly, 1 mg/mL of raw LV soot was mixed into a solution of 2 mg/mL of PFO-BPy in toluene. This solution was then sonicated with a 1/2 in. probe tip for 30 min at 300 W (Cole-Parmer CPX 750) in a bath of cool (18 °C) flowing water for heat dissipation. After sonication, solutions were centrifuged at 30 000*g* for 5 min using a SW32-Ti rotor (Beckman).

Sample Preparation. Polymer-embedded SWCNTs were fabricated using an ebeam evaporator to coat a 100 nm layer of Au on top of a standard p++ type Si wafer with a 90 nm SiO_2 layer. This was followed by a 160 nm layer of spin-coated polystyrene. PFO-BPy-dispersed LV SWCNTs in toluene were deposited directly onto the first layer of polymer and then covered with a second layer of PS. Finally, the PS samples were baked at 105 °C for several hours before cryogenic measurements to remove charge trap states.[29,62]

Microphotoluminescence Setup. Measurements of microphotoluminescence were taken inside a liquid helium cryostat with a 9 K base temperature. Samples were excited with a laser diode operating at 780 nm in continuous wave or pulsed mode (80 MHz repetition rate and 100 ps pulse length). The laser wavelength was tuned for up to 4 nm (8 meV) by adjusting the temperature of the laser system. A laser spot size of about 1.5 μm was achieved using a microscope objective with numerical aperture of 0.55. The relative position between sample and laser spot was adjusted with a piezoelectric *xyz* actuator (attocube) mounted directly onto the coldfinger of the cryostat. Spectral emission was dispersed by a 0.75 m focal length spectrometer and imaged by a silicon-based CCD camera. Laser stray light was rejected by a 780 nm notch filter and 800 nm high-pass filter. To enhance the exciton absorption, the laser polarization was rotated with a half-wave plate along the tube axis.

Conflict of Interest: The authors declare no competing financial interest.

Acknowledgment. The authors like to thank Christophe Galland, Alexander Hoegele, Christophe Voisin, and Jean-Sebastien Lauret for fruitful discussions. S.S. acknowledges financial support by the National Science Foundation (NSF), CAREER award ECCS-1053537. J.B. and K.M. gratefully acknowledge funding from the Solar Photochemistry Program of the U.S. Department of Energy, Office of Science, Basic Energy Sciences, Division of Chemical Sciences, Geosciences and Biosciences, under Contract No. DE-AC36-08GO28308 to NREL. This research effort used microscope resources partially funded by NSF through Grant DMR-0922522. Sample fabrication was carried out in part at the Center for Functional Nanomaterials, Brookhaven National Laboratory, which is supported by the U.S. Department of Energy, Office of Basic Energy Sciences, under Contract No. DE-AC02-98CH10886.

Supporting Information Available: Further details of the Ohmic and non-Ohmic theory models, the temperature dependence of PL spectra, and results for SDBS dispersed LV-grown SWCNTs are provided. The Supporting Information is available free of charge on the ACS Publications website at DOI: 10.1021/acsnano.5b01997.

REFERENCES AND NOTES

1. Avouris, P.; Freitag, M.; Perebeinos, V. Carbon-Nanotube Photonics and Optoelectronics. *Nat. Photonics* **2008**, 341–350.
2. Dresselhaus, M. S.; Dresselhaus, G.; Saito, R.; Jario, A. Exciton Photophysics of Carbon Nanotubes. *Annu. Rev. Phys. Chem.* **2007**, *58*, 719–747.
3. Högele, A.; Galland, C.; Winger, M.; Imamoglu, A. Photon Antibunching in the Photoluminescence Spectra of a Single Carbon Nanotube. *Phys. Rev. Lett.* **2008**, *100*, 217401/1–217401/4.
4. Walden-Newman, W.; Sarpkaya, I.; Strauf, S. Quantum Light Signatures and Nanosecond Spectral Diffusion from Cavity-Embedded Carbon-Nanotubes. *Nano Lett.* **2012**, *12*, 1934–1941.
5. Wang, F.; Dukovic, G.; Brus, L. E.; Heinz, T. F. The Optical Resonances in Carbon Nanotubes Arise from Excitons. *Science* **2005**, *308*, 838–841.
6. Tsyboulski, D. A.; Rocha, J.-D. R.; Bachilo, S. M.; Cognet, L.; Weisman, R. B. Structure-Dependent Fluorescence Efficiencies of Individual Single Walled Carbon Nanotubes. *Nano Lett.* **2007**, *7*, 3080–3085.
7. Siitonen, A. J.; Tsyboulski, D. A.; Bachilo, S. M.; Weisman, R. B. Surfactant-Dependent Exciton Mobility in Single-Walled Carbon Nanotubes Studied by Single-Molecule Reactions. *Nano Lett.* **2010**, *10*, 1595–1599.
8. Hertel, T.; Himmelein, S.; Ackermann, T.; Stich, D.; Crochet, J. Diffusion Limited Photoluminescence Quantum Yields in 1-D Semiconductors: Single-Wall Carbon Nanotubes. *ACS Nano* **2010**, *4*, 7161–7168.
9. Lee, J. A.; Wang, X.; Carlson, L. J.; Smyder, J. A.; Loesch, B.; Tu, X.; Zheng, M.; Krauss, T. D. Bright Fluorescence from Individual Single-Walled Carbon Nanotubes. *Nano Lett.* **2011**, *11*, 1636–1640.
10. Harrah, D. M.; Swan, A. K. The Role of Length and Defects on Optical Quantum Efficiency and Exciton Decay Dynamics in Single-Walled Carbon Nanotubes. *ACS Nano* **2011**, *5*, 647–655.
11. Blackburn, J. L.; et al. Protonation Effects on the Branching Ratio in Photoexcited Single-Walled Carbon Nanotube Dispersions. *Nano Lett.* **2008**, *8*, 1047–1054.
12. Larsen, B. A.; Deria, P.; Holt, J. M.; Stanton, I. N.; Heben, M. J.; Therien, M. J.; Blackburn, J. L. Effects of Solvent Polarity and Electrophilicity on Quantum Yields and Solvatochromic Shifts of Single-Walled Carbon Nanotube Photoluminescence. *J. Am. Chem. Soc.* **2012**, *134*, 12485–12491.
13. Finnie, P.; Levebvre, J. Photoinduced Band Gap Shift and Deep Levels in Luminescent Carbon Nanotubes. *ACS Nano* **2012**, *6*, 1702–1714.
14. Crochet, A. J.; Duque, J. G.; Werner, J. H.; Doorn, S. K. Photoluminescence Imaging of Electronic-Impurity-Induced Exciton Quenching in Single-Walled Carbon Nanotubes. *Nat. Nanotechnol.* **2012**, *7*, 126–132.
15. Berger, S.; Voisin, C.; Cassabois, G.; Delalande, C.; Roussignol, P.; Marie, X. Temperature Dependence of Exciton Recombination in Semiconducting Single-Wall Carbon Nanotubes. *Nano Lett.* **2007**, *7*, 398–402.
16. Hagen, A.; Steiner, M.; Raschke, M. B.; Lienau, C.; Hertel, T.; Qian, H.; Meixner, A. J.; Hartschuh, A. Exponential Decay Lifetimes of Exciton in Individual Single-Walled Carbon Nanotubes. *Phys. Rev. Lett.* **2005**, *95*, 197401.
17. Sarpkaya, I.; Zhang, Z.; Walden-Newman, W.; Wang, X.; Hone, J.; Wong, C. W.; Strauf, S. Prolonged Spontaneous Emission and Dephasing of Localized Excitons in Air-Bridged Carbon Nanotubes. *Nat. Commun.* **2013**, *4*, 2152.
18. Deshpande, V. V.; Chandra, B.; Caldwell, R.; Novikov, D. S.; Hone, J.; Bockrath, M. Mott Insulating State in Ultraclean Carbon Nanotubes. *Science* **2009**, *323*, 106–110.
19. Deshpande, V. V.; Bockrath, M. The One-Dimensional Wigner Crystal in Carbon Nanotubes. *Nat. Phys.* **2008**, *4*, 314–318.

20. Kuemmeth, F.; Ilani, S.; Ralph, D. C.; McEuen, P. L. Coupling of Spin and Orbital Motion of Electrons in Carbon Nanotubes. *Nature* **2008**, *452*, 448–452.
21. Hofmann, M. S.; Glückert, J. T.; Noé, J.; Bourjau, C.; Dehmel, R.; Högele, A. Bright, Long Lived and Coherent Excitons in Carbon Nanotube Quantum Dots. *Nat. Nanotechnol.* **2013**, *8*, 502–505.
22. Spataru, C. D.; Ismail-Beigi, S.; Capaz, R. B.; Louie, S. G. Theory and Ab Initio Calculation of Radiative Lifetime of Excitons in Semiconducting Carbon Nanotubes. *Phys. Rev. Lett.* **2005**, *95*, 247402.
23. Perebeinos, V.; Tersoff, J.; Avouris, P. Radiative Lifetime of Excitons in Carbon Nanotubes. *Nano Lett.* **2005**, *5*, 2495–2499.
24. Ma, Y.-Z.; Graham, M. W.; Fleming, G. R.; Green, A. A.; Hersam, M. C. Ultrafast Exciton Dephasing in Semiconducting Single-Walled Carbon Nanotubes. *Phys. Rev. Lett.* **2008**, *101*, 217402.
25. Graham, M. W.; Ma, Y.-Z.; Green, A. A.; Hersam, M. C.; Fleming, G. R. Pure Optical Dephasing Dynamics in Semiconducting Single-Walled Carbon Nanotubes. *J. Chem. Phys.* **2011**, *134*, 034504.
26. Galland, C.; Hogele, A.; Tureci, H. E.; Imamoglu, A. Non-Markovian Decoherence of Localized Nanotube Excitons by Acoustic Phonons. *Phys. Rev. Lett.* **2008**, *101*, 067402.
27. Nguyen, D. T.; Voisin, C.; Roussignol, Ph.; Roquelet, C.; Lauret, J. S.; Cassabois, G. Phonon-Induced Dephasing in Single-Wall Carbon Nanotubes. *Phys. Rev. B* **2011**, *84*, 115463.
28. Vialla, F.; Chassagneux, Y.; Ferreira, R.; Roquelet, C.; Diederichs, C.; Cassabois, G.; Roussignol, Ph.; Lauret, J. S.; Voisin, C. Unifying the Low-Temperature Photoluminescence Spectra of Carbon Nanotubes: The Role of Acoustic Phonon Confinement. *Phys. Rev. Lett.* **2014**, *113*, 057402/1–057402/5.
29. Ai, N.; Walden-Newman, W.; Song, Q.; Kalliakos, S.; Strauf, S. Suppression of Blinking and Enhanced Exciton Emission from Individual Carbon Nanotubes. *ACS Nano* **2011**, *5*, 2664–2670.
30. Alexander-Webber, J. A.; Faugeras, C.; Kossacki, P.; Potemski, M.; Wang, X.; Kim, H. D.; Stranks, S. D.; Taylor, R. A.; Nicholas, R. J. Hyperspectral Imaging of Exciton Photoluminescence in Individual Carbon Nanotubes Controlled by High Magnetic Fields. *Nano Lett.* **2014**, *14*, 5194–5200.
31. Chou, S. G.; et al. Phonon-Assisted Excitonic Recombination Channels Observed in DNA-Wrapped Carbon Nanotubes Using Photoluminescence Spectroscopy. *Phys. Rev. Lett.* **2005**, *94*, 127402.
32. Ates, S.; Ulrich, S. M.; Ulhaq, A.; Reitzenstein, S.; Löffler, A.; Höfling, S.; Forchel, A.; Michler, P. Non-resonant Dot-Cavity Coupling and Its Potential for Resonant Single-Quantum-Dot Spectroscopy. *Nat. Photonics.* **2009**, *3*, 724–728.
33. Strauf, S.; Jahnke, F. Single Quantum Dot Nanolaser. *Laser Photonics Rev.* **2011**, *5*, 607–633.
34. Jorio, A.; et al. Linewidth of the Raman Features of Individual Single-Wall Carbon Nanotubes. *Phys. Rev. B* **2002**, *66*, 115411.
35. Chatzakis, I.; Yan, H.; Song, D.; Berciaud, S.; Heinz, T. F. Temperature Dependence of the Anharmonic Decay of Optical Phonons in Carbon Nanotubes and Graphite. *Phys. Rev. B* **2011**, *83*, 205411.
36. Ikeda, K.; Uosaki, K. Coherent Phonon Dynamics in Single-Walled Carbon Nanotubes Studied by Time-Frequency Two-Dimensional Coherent Anti-Stokes Raman Scattering Spectroscopy. *Nano Lett.* **2009**, *9*, 1378–1381.
37. Kim, J. H.; Yee, K.-J.; Lim, Y.-S.; Booshehri, L. G.; Hároz, E. H.; Kono, J. Dephasing of G-Band Phonons in Single-Wall Carbon Nanotubes Probed *via* Impulsive Stimulated Raman Scattering. *Phys. Rev. B* **2012**, *86*, 161415(R).
38. Tan, P. H.; Rozhin, A. G.; Hasan, T.; Hu, P.; Scardaci, V.; Milne, W. I.; Ferrari, A. C. Photoluminescence Spectroscopy of Carbon Nanotube Bundles: Evidence for Exciton Energy Transfer. *Phys. Rev. Lett.* **2007**, *99*, 137402.
39. Htoon, H.; O'Connell, M. J.; Doorn, S. K.; Klimov, V. Single Carbon Nanotubes Probed by Photoluminescence Excitation Spectroscopy: The Role of Phonon-Assisted Transitions. *Phys. Rev. Lett.* **2005**, *94*, 127403.
40. Htoon, H.; O'Connell, M.; Cox, P.; Doorn, S.; Klimov, V. Low Temperature Emission Spectra of Individual Single-Walled Carbon Nanotubes: Multiplicity of Subspecies within Single-Species Nanotube Ensembles. *Phys. Rev. Lett.* **2004**, *93*, 027401.
41. Cheng, Y.; Zhou, S.; Zhu, B. Isotope Effect on Phonon Spectra in Single-Wall Carbon Nanotubes. *Phys. Rev. B* **2005**, *72*, 035410.
42. Cronin, S. B.; Swan, A. K.; Unlü, M. S.; Goldberg, B. B.; Dresselhaus, M. S.; Tinkham, M. Resonant Raman Spectroscopy of Individual Metallic and Semiconducting Single-Wall Carbon Nanotubes Under Uniaxial Strain. *Phys. Rev. B* **2005**, *72*, 035425.
43. Souza Filho, A. G.; et al. Effect of Quantized Electronic States on the Dispersive Raman Features in Individual Single-Wall Carbon Nanotubes. *Phys. Rev. B* **2001**, *65*, 035404.
44. Engtrakul, C.; Davis, M. F.; Mistry, K.; Larsen, B. A.; Dillon, A. C.; Heben, M. J.; Blackburn, J. L. Solid-State ^{13}C NMR Assignment of Carbon Resonances on Metallic and Semiconducting Single-Walled Carbon Nanotubes. *J. Am. Chem. Soc.* **2010**, *132*, 9956–9957.
45. Mistry, K. S.; Larsen, B. A.; Bergeson, J. D.; Barnes, T. M.; Teeter, G.; Engtrakul, C.; Blackburn, J. L. n-Type Transparent Conducting Films of Small Molecule and Polymer Amine Doped Single-Walled Carbon Nanotubes. *ACS Nano* **2011**, *5*, 3714–3723.
46. Blackburn, J. L.; Holt, J. M.; Irurzun, V. M.; Resasco, D. E.; Rumbles, G. Confirmation of K-Momentum Dark Exciton Vibronic Sidebands Using ^{13}C-Labeled, Highly Enriched (6,5) Single-Walled Carbon Nanotubes. *Nano Lett.* **2012**, *12*, 1398–1403.
47. Fischer, J.; Trauzettel, B.; Loss, D. Hyperfine Interaction and Electron-Spin Decoherence in Graphene and Carbon Nanotube Quantum Dots. *Phys. Rev. B* **2009**, *80*, 155401.
48. Chekhovich, E. A.; Makhonin, M. N.; Tartakovskii, A. I.; Yacoby, A.; Bluhm, H.; Nowack, K. C.; Vandersypen, L. M. K. Nuclear Spin Effects in Semiconductor Quantum Dots. *Nat. Mater.* **2013**, *12*, 494.
49. Pennington, G.; Goldsman, N. Low-Field Semiclassical Carrier Transport in Semiconducting Carbon Nanotubes. *Phys. Rev. B* **2005**, *71*, 205318.
50. Georgi, C.; Hartmann, N.; Gokus, T.; Green, A. A.; Hersam, M. C.; Hartschuh, A. Photoinduced Luminescence Blinking and Bleaching in Individual Single-Walled Carbon Nanotubes. *ChemPhysChem* **2008**, *9*, 1460–1464.
51. Finnie, P.; Levebvre, J. Photoinduced Band Gap Shift and Deep Levels in Luminescent Carbon Nanotubes. *ACS Nano* **2012**, *6*, 1702–1714.
52. Santos, S. M.; Yuma, B.; Berciaud, S.; Shaver, J.; Gallart, M.; Gilliot, P.; Cognet, L.; Lounis, B. All-Optical Trion Generation in Single-Walled Carbon Nanotubes. *Phys. Rev. Lett.* **2011**, *107*, 187401.
53. Harutyunyan, H.; Gokus, T.; Green, A. A.; Hersam, M. C.; Allegrini, M.; Hartschuh, A. Defect-Induced Photoluminescence from Dark Excitonic States in Individual Single-Walled Carbon Nanotubes. *Nano Lett.* **2009**, *9*, 2010–2014.
54. Piao, Y.; Meany, B.; Powell, L. R.; Valley, N.; Kwon, H.; Schatz, G. C.; Wang, Y. Brightening of Carbon Nanotube Photoluminescence through the Incorporation of sp^3 Defects. *Nat. Chem.* **2013**, *5*, 840–845.
55. Ma, X.; Adamska, L.; Yamaguchi, H.; Yalcin, S. E.; Tretiak, S.; Doorn, S. K.; Htoon, H. Electronic Structure and Chemical Nature of Oxygen Dopant States in Carbon Nanotubes. *ACS Nano* **2014**, *8*, 10782–10789.
56. Strauf, S.; Michler, P.; Klude, M.; Hommel, D.; Bacher, G.; Forchel, A. Quantum Optical Studies on Individual Acceptor Bound Excitons in a Semiconductor. *Phys. Rev. Lett.* **2002**, *89*, 177403.

57. Strauf, S.; Michler, P.; Klude, M.; Hommel, D.; Bacher, G.; Forchel, A. *Proceedings of the 26th International Conference on the Physics of Semiconductors*, Edinburgh, Institute of Physics Conference Series Number 171, **2002**; ISBN 0-7503-0924-5.
58. Hwang, J.-Y.; Nish, A.; Doig, J.; Douven, S.; Chen, C.-W.; Chen, L.-C.; Nicholas, R. J. Polymer Structure and Solvent Effects on the Selective Dispersion of Single-Walled Carbon Nanotubes. *J. Am. Chem. Soc.* **2008**, *130*, 3543–3553.
59. Gomulya, W.; Gao, J.; Loi, M. A. Conjugated Polymer-Wrapped Carbon Nanotubes: Physical Properties and Device Applications. *Eur. Phys. J. B* **2013**, *86*, 404.
60. Mistry, K. S.; Larsen, B. A.; Blackburn, J. L. High-Yield Dispersions of Large-Diameter Semiconducting Single-Walled Carbon Nanotubes with Tunable Narrow Chirality Distributions. *ACS Nano* **2013**, *7*, 2231–2239.
61. Stürzl, N.; Lebedkin, S.; Malik, S.; Manfred, M. K. Preparation of ^{13}C Single-Walled Carbon Nanotubes by Pulsed Laser Vaporization. *Phys. Status Solidi B* **2009**, *246*, 2465–2468.
62. Kim, W.; Javey, A.; Vermesh, O.; Wang, Q.; Li, Y.; Dai, H. Hysteresis Caused by Water Molecules in Carbon Nanotube Field-Effect Transistors. *Nano Lett.* **2003**, *3*, 193–198.